The Astrophysical Journal, 580:1149–1158, 2002 December 1

A SUBARU/HIGH DISPERSION SPECTROGRAPH STUDY OF LEAD (Pb) ABUNDANCES IN EIGHT *s*-PROCESS ELEMENT–RICH, METAL-POOR STARS[1]

Wako Aoki,[2] Sean G. Ryan,[3] John E. Norris,[4] Timothy C. Beers,[5] Hiroyasu Ando,[2] and Stelios Tsangarides[3]

Received 2002 April 19; accepted 2002 August 5

ABSTRACT

We report the abundances of neutron-capture elements in eight carbon-rich, metal-poor ($-2.7 \leq$ [Fe/H] ≤ -1.9) stars observed with the Subaru Telescope High Dispersion Spectrograph. The derived abundance patterns indicate that the neutron-capture elements in these objects primarily originated from *s*-process nucleosynthesis, although the [Ba/Eu] abundance ratios in some objects are lower than that of the solar system *s*-process component. The present analysis has yielded the Pb abundances for seven objects as well as an upper limit for one object from use of the Pb I λ4057 and λ3683 lines. The values of [Pb/Ba] in these objects cover a wide range, between -0.3 and 1.2. Theoretical studies of *s*-process nucleosynthesis at low metallicity are required to explain this large dispersion of the [Pb/Ba] values. Variations in radial velocity have been found for two of the eight objects, suggesting that, at least in these instances, the observed excess of *s*-process elements is due to the transfer of material across a binary system including an AGB star. Comparisons with predictions of AGB nucleosynthesis models are discussed.

Subject headings: nuclear reactions, nucleosynthesis, abundances — stars: abundances — stars: AGB and post-AGB — stars: carbon — stars: Population II

On-line material: machine-readable table

1. INTRODUCTION

Lead (Pb) isotopes form, along with those of bismuth, the group of the heaviest stable nuclei. Understanding of the physical processes responsible for the synthesis of these nuclei, as well as their enrichment history in the Galaxy, is important in the study of stellar nucleosynthesis and Galactic chemical evolution as well as for precision cosmochronology since these nuclei are the expected decay products of Th and U (Goriely & Arnould 2001; Schatz et al. 2002). The majority of Pb nuclei in the solar system are believed to have originated in the *s*-process. However, the so-called main component of the *s*-process in classical models cannot explain the solar system abundances of Pb; hence, another component (the so-called strong component) was introduced (see, e.g., Käppeler, Beer, & Wisshak 1989). Recent theoretical work on nucleosynthesis in asymptotic giant branch (AGB) stars, based on the idea of an *s*-process that occurs in the radiative zone during the interpulse phase, has predicted large production of Pb and Bi ($Z = 82$ and 83, respectively) compared to lighter *s*-process elements such as Sr ($Z = 38$) and Ba ($Z = 56$) in low-metallicity AGB stars (Gallino et al. 1998; Goriely & Mowlavi 2000; Busso et al. 2001). These works suggested that the Pb production in low-metallicity AGB stars corresponds to the strong component assumed in the classical models. Studies of Pb enrichment in the Galaxy have also started using the yields predicted by these AGB models (Travaglio et al. 2001).

Recent abundance studies of *s*-process element–enhanced, metal-poor stars, based on high-resolution spectroscopy, have measured the abundances of Pb and other neutron-capture elements in a number of stars and made it possible to examine the models of AGB nucleosynthesis in greater detail. For instance, Aoki et al. (2000) determined the abundances of 16 neutron-capture elements, including Pb, for the *s*-process element–rich, very metal-poor ([Fe/H] $= -2.7$) star LP 625-44.[6] The Pb abundance of this object is, however, much *lower* than the prediction by the "standard" model of Gallino et al. (1998), when the abundance pattern is normalized by the abundance of lighter *s*-process nuclei (e.g., Ba). A similar result was derived for another metal-poor star, LP 706-7, by Aoki et al. (2001). Their abundances could, however, be reconciled with the models of Gallino et al. if the extent of the ^{13}C pocket is reduced by a factor of $\simeq$24 (Ryan et al. 2001). On the other hand, van Eck et al. (2001) studied another three *s*-process element–enhanced, metal-poor objects and found very *large* Pb enhancements in these objects compared to those of the lighter elements. They concluded that the results can be explained well by the model of AGB nucleosynthesis presented by Goriely & Mowlavi (2000).

Thus, the abundance ratios of the Pb and the neutron-capture elements at the second peak of the *s*-process ($Z \sim 56$) produced by metal-deficient AGB stars seem to show a large dispersion or might even be classified into two distinct groups. In order to understand the nature of the *s*-process nucleosynthesis at low metallicity, we have embarked on an extensive set of studies of the neutron-capture elements for metal-poor stars with excesses of

[1] Based on data collected at the Subaru Telescope, which is operated by the National Astronomical Observatory of Japan.

[2] National Astronomical Observatory, Mitaka, Tokyo 181-8588, Japan; aoki.wako@nao.ac.jp, ando@optik.mtk.nao.ac.jp.

[3] Department of Physics and Astronomy, Open University, Walton Hall, Milton Keynes MK7 6AA, UK; s.g.ryan@open.ac.uk, s.tsangarides@open.ac.uk.

[4] Research School of Astronomy and Astrophysics, Australian National University, Mount Stromlo Observatory, Cotter Road, Weston, ACT 2611, Australia; jen@mso.anu.edu.au.

[5] Department of Physics and Astronomy, Michigan State University, East Lansing, MI 48824-1116; beers@pa.msu.edu.

[6] $[A/B] = \log(N_A/N_B) - \log(N_A/N_B)_\odot$ and $\log \epsilon_A = \log(N_A/N_H) + 12$ for elements A and B.

s-process elements. In this paper we report the abundances of neutron-capture elements, including Pb, for eight metal-poor stars.

2. OBSERVATIONS AND MEASUREMENTS

We selected our program sample from the list of metal-poor stars provided by the HK survey of Beers and collaborators (Beers, Preston, & Shectman 1992; Beers 1999; Norris, Ryan, & Beers 1999), taking account of the metallicity and apparent level of carbon enhancement (as indicated by an index, *GP*, that measures the strength of the CH *G* band at 4300 Å). We have observed more than 10 stars and selected the seven stars that clearly exhibit excesses of the *s*-process elements. For purposes of comparison, we have also observed the *s*-process element–rich star HD 196944 studied by van Eck et al. (2001).

Observations were carried out with the High Dispersion Spectrograph (HDS) of the 8.2 m Subaru Telescope (Noguchi et al. 2002). Program stars and observational details are provided in Table 1. We note that CS 31062-012 is identical to LP 706-7, previously studied by Norris et al. (1997) and Aoki et al. (2001). The spectra were taken with a resolving power $R = 50,000$, except for HD 196944, for which an $R = 90,000$ spectrum was obtained. Our spectra cover the wavelength range 3550–5250 Å. Signal-to-noise ratios (S/Ns) per 0.012 Å pixel at 4000 Å are given in the table as well. Data reduction was performed in the standard way within the IRAF[7] environment, following Aoki et al. (2002b).

Equivalent widths for isolated lines were measured by fitting Gaussian profiles to the absorption lines. The line list and equivalent widths measured are presented in Table 2.

The radial velocity (V_r) measured for our spectra are also presented in Table 1. Our separate measurement of the radial velocity for CS 29526−110 ($V_r = 201.70 \pm 0.26$ km s^{-1} at JD = 2,452,152.7) using the William Herschel Telescope Utrecht echelle spectrograph shows a variation of the radial velocity, suggesting binarity for this object. The radial velocities measured for our Subaru/HDS spectra of CS 22880−027 and CS 22898−027 agree with the averages of the results by Preston & Sneden (2001) to within 1 km s^{-1}.

[7] IRAF is distributed by the National Optical Astronomy Observatories, which is operated by the Association of Universities for Research in Astronomy, Inc., under cooperative agreement with the National Science Foundation.

3. ABUNDANCE ANALYSIS

A standard analysis, using the model atmospheres of Kurucz (1993) and the equivalent widths measured above was performed for lines of Fe I and Fe II and most of the neutron-capture elements. A spectrum synthesis technique was applied to the molecular bands of CH, C_2, and CN in order to determine the carbon and nitrogen abundances, which are required for estimates of the effective temperature. The line broadening due to macroturbulence in the stellar atmospheres, and from the spectrograph itself, was estimated from the clean Fe lines for each object and then applied to the spectrum synthesis.

The effective temperatures given in Table 3 were estimated from broadband colors using previously derived temperature scales. For most of our program stars, we applied the temperature scale based on the dereddened $(B-V)_0$ color for carbon-rich, metal-poor stars produced by Aoki et al. (2002a). The $B-V$ color of CS 30301−015 is uncertain; hence, we assume a larger uncertainty in effective temperature in the error estimation procedure described below. The effective temperature of CS 22942−019 was redetermined after its carbon and nitrogen abundances were estimated because abundances for these two elements assumed in the first determination of the effective temperature were found to be too low and the effect of molecular absorption was not included correctly. *JHK* photometry data from the interim release of the 2MASS Point Source Catalog (Skrutskie et al. 1997) are also available for three stars (CS 29526−110, CS 22898−027, and CS 31062−050). After correcting for reddening, the effective temperature scale based on $(V-K)_0$ by Alonso, Arribas, & Martínez-Roger (1996) was applied and yielded consistent results with those obtained from $(B-V)_0$ colors. The difference between the two effective temperatures is rather large in CS 29526−110: the effective temperature estimated from $(V-K)_0$ is higher by 200 K than that from $(B-V)_0$. We assume a larger uncertainty of $T_{\rm eff}$ for this object in the error estimates below.

Surface gravities for our program stars were determined from the ionization balance between Fe I and Fe II, the metallicities were estimated from the abundance analysis for these lines, and the microturbulence was determined from the Fe I lines by demanding no dependence of the derived abundance on equivalent widths. The results are provided in Table 3. While the effective temperature of CS 29526−110 is the highest in our sample and suggests that this star might be a main-sequence turn-off star, its gravity ($\log g = 3.2$) is not particularly high. This may be due to

TABLE 1
PROGRAM STARS AND OBSERVATIONS

Star	V	$B-V$	$E(B-V)$	GP	Exposure Time[a] (min)	S/N	V_r (km s^{-1})	Observation Date (JD)
CS 22942−019 ..	12.71	0.86	0.02	7.60	60 (2)	61	−232.88 ± 0.40	2000 Aug 20 (2451778)
CS 29526−110 ..	13.37	0.35	0.00	1.94	90 (3)	62	208.35 ± 0.76	2001 Jan 28 (2,451,938)
CS 22898−027 ..	12.76	0.50	0.03	4.71	60 (3)	49	−47.90 ± 0.47	2001 Jul 22 (2,452,113)
HD 196944.....	8.41	0.61	0.00	...	20 (1)	150	−174.76 ± 0.36	2001 Jul 25 (2,452,116)
CS 31062−012 ..	12.10	0.46	0.00	3.67	25 (1)	57	80.76 ± 0.37	2001 July 25 (2,452,117)
CS 31062−050 ..	13.04	0.64	0.02	6.41	50 (2)	47	7.75 ± 0.67	2001 July 25 (2,452,117)
CS 30301−015 ..	...	0.99:	...	7.88	50 (2)	53	86.46 ± 0.43	2001 July 25 (2,452,116)
CS 22880−074 ..	13.27	0.57	0.04	5.71	60 (2)	42	59.57 ± 0.48	2001 Jul 25 (2,452,116)

[a] Number of exposures in parentheses.

TABLE 2

EQUIVALENT WIDTHS

Wavelength (Å)	LEP (eV)	log *gf*	29526−110	22898−027	31062−012	22880−074	31062−050	HD 196944	22942−019	30301−015
					Sr II					
4077.71	0.00	0.15	102.3	115.4	76.6	127.6	146.9	179.7	488:†	176:†
4161.80	2.94	−0.50	...	...	...	...	...	16.1	...	...
4215.52	0.00	−0.17	90.3	97.8	56.2	104.6	127.2	184.7	364:†	...
					Y II					
3600.73	0.18	0.28	...	48.6	...	...	...	95.4*	...	...
3611.04	0.13	0.01	...	...	...	34.2	...	86.0*	...	...
3628.70	0.13	−0.71[a]	...	...	...	...	...	58.7*	...	...
3788.69	0.10	−0.06	...	...	...	...	...	96.8	...	...
3950.35	0.10	−0.49	...	25.0	7.6	30.2	...	78.7	101.0	...
4682.32	0.41	−1.51[a]	...	...	...	...	...	22.8	...	...
4883.68	1.08	0.07	...	...	...	...	...	56.2	103.1	61.2
5087.42	1.08	−0.16	...	...	...	...	...	42.7	...	55.2
5200.41	0.99	−0.57	...	...	...	...	...	36.6	...	33.0
5205.72	1.03	−0.34	...	...	...	...	...	35.7	...	41.8
					Zr II					
3573.08	0.32	−1.04	...	...	...	...	...	33.5	...	...
3630.02	0.35	−1.11	...	...	...	...	...	25.1	...	...
3998.97	0.56	−0.67	...	...	...	...	...	51.2	75.4	...
4029.68	0.71	−0.76	...	8.0	...	...	23.6	41.9	...	...
4050.33	0.71	−1.00	...	...	...	...	...	...	59.2	...
4149.20	0.80	−0.03	28.7	...	...	...	...	...	...	...
4208.98	0.71	−0.46	...	16.9	...	...	31.9	47.0	...	...
4258.05	0.56	−1.13	...	...	...	...	...	29.9	...	...
4443.00	1.49	−0.33	...	...	...	...	...	...	56.4	...
					Ba II					
3891.78	2.51	0.28[b]	...	49.5	...	...	...	34.0	50.7†	...
4130.65	2.72	0.56[c]	50.2	64.3	23.1	31.0†	85.2	49.1	69.4†	81.7
4166.00	2.72	−0.41	12.7†	15.1	...	...	27.7	11.5	22.1†	...
					La II					
3790.83	0.13	0.03	...	...	...	...	70.7	...	...	...
3949.10	0.40	0.49	69.0	107.9	34.4	50.4	129.1*	95.1	...	...
3988.52	0.40	0.21	44.3	...	...	33.3	120.9*	67.9	...	70.3
3995.75	0.17	−0.06	34.3	59.5	18.6	...	89.4*	54.2	60.4	73.1
4086.72	0.00	−0.07	...	54.3	...	33.0	73.7	...	61.1	...
4123.23	0.32	0.13	40.3	...	19.1	...	74.2	50.9	...	...
4322.51	0.17	−0.93	...	20.7	...	...	51.7	15.8	...	...
4333.74	0.17	−0.06	54.1	...	...	...	...	...	...	...
4429.90	0.23	−0.35	36.5	...	...	...	...	47.6	...	...
4662.51	0.00	−1.24	...	14.4	...	...	...	...	...	32.7
					Ce II					
3853.16	0.00	−0.36[d]	...	21.5	...	...	...	...	...	...
3909.31	0.45	−0.52	...	...	...	...	19.3	9.0	...	...
3940.34	0.32	−0.20[d]	...	16.6	...	...	25.8	24.7	...	30.1
3942.75	0.86	0.41[d]	...	24.8	...	...	...	23.9	...	33.7
3960.91	0.32	−0.20	...	...	...	...	...	15.4	...	...
3980.88	0.71	0.03	...	...	...	...	...	12.0	...	...
3984.68	0.96	0.41	...	...	...	...	...	15.2	...	...
3992.39	0.45	−0.13[d]	...	10.4	...	...	...	...	...	...
3999.24	0.29	0.32[d]	...	...	8.5	17.5	45.6	32.0	39.8	53.0
4014.90	0.53	0.05[d]	...	12.3	...	...	34.8	...	...	...
4046.34	0.55	−0.11[d]	...	8.9	...	...	...	15.8	...	...
4053.51	0.00	−0.60[d]	...	...	...	...	26.1	17.7	23.8	...
4068.84	0.70	−0.13[d]	...	...	...	...	...	16.6	...	...
4072.92	0.33	−0.71	...	11.0	...	...	...	14.7	...	...
4073.48	0.48	0.28[d]	...	27.2	...	19.9	35.6	31.7	...	...
4118.14	0.70	0.10[d]	...	...	...	...	37.9	23.9	...	...

TABLE 2—*Continued*

Wavelength (Å)	LEP (eV)	log *gf*	29526−110	22898−027	31062−012	22880−074	31062−050	HD 196944	22942−019	30301−015
4120.83	0.32	−0.51[d]	...	...	...	...	...	19.4	...	...
4124.79	0.68	−0.10[d]	...	...	...	...	30.7	...	...	...
4127.37	0.68	0.19[d]	...	...	...	...	37.1	...	...	...
4137.65	0.52	0.32[d]	...	34.8	11.3	...	49.9	39.2	...	59.3
4145.00	0.70	0.03[d]	...	...	...	...	...	14.6	20.5	...
4165.61	0.91	0.51[d]	...	22.8	...	...	38.4	28.8	...	...
4185.33	0.42	−0.56	...	...	...	...	...	10.6	...	...
4193.87	0.55	−0.40[d]	...	...	...	...	18.5	14.0	...	...
4222.60	0.12	−0.21[d]	...	28.9	8.8	...	44.6	33.5	...	58.1
4349.79	0.53	−0.19[d]	...	...	...	...	25.6	...	...	...
4418.78	0.86	0.26[d]	12.7	23.9	...	...	...	30.4	...	...
4449.34	0.61	−0.11[d]	...	21.6	...	...	...	25.2	...	...
4460.21	0.48	0.25[d]	...	35.1	...	...	...	40.0	...	77.8
4471.24	0.70	0.23[d]	...	...	10.6	...	44.9	33.4	...	...
4483.90	0.86	0.09	...	...	...	...	...	...	47.1	...
4486.91	0.29	−0.39[d]	...	18.6	...	...	39.7	31.7	35.5	46.1
4551.30	0.74	−0.49	...	...	...	...	19.2	...	...	24.5
4560.28	0.91	0.08[d]	...	17.4	...	...	37.3	19.9	...	53.6
4560.96	0.68	−0.47	...	...	...	...	22.7	9.2	...	23.7
4562.36	0.48	0.16[d]	...	...	9.9	18.8	57.5	36.0	49.0	70.5
4593.93	0.70	−0.03[d]	...	19.0	11.9	...	49.6	19.9	...	55.8
4628.16	0.52	0.09[d]	...	18.6	10.2	...	48.5	29.2	...	57.4
5187.45	1.21	0.16[d]	...	...	...	...	...	...	...	14.2
					Nd II					
3780.40	0.47	−0.27	...	...	...	...	...	25.2	...	...
3784.25	0.38	0.23	...	34.1	7.0	...	...	30.7	28.8	...
3911.17	0.47	0.20	...	...	...	...	52.2	27.6	...	...
3927.10	0.18	−0.52	...	...	...	...	33.0	...	18.2	...
3941.51	0.15	0.06	...	...	14.8	...	...	36.5	...	...
3979.49	0.20	−0.11	...	...	...	...	...	29.5	30.1	...
3991.74	0.00	−0.40	...	28.9	...	...	54.8	33.0	50.8	...
4012.70	0.00	−0.64	...	...	...	...	36.3	18.0	20.8	...
4020.87	0.32	−0.18	...	...	...	...	47.1	29.1	47.1	...
4021.34	0.32	0.24	...	...	7.3	...	43.2	21.3	...	...
4023.00	0.20	−0.19	...	23.4	...	...	50.8	18.5	...	...
4038.12	0.18	−0.78	...	...	...	...	44.4	...	...	...
4051.15	0.38	−0.21	...	19.9	...	...	34.5	...	...	...
4059.96	0.20	−0.33	...	...	...	...	...	...	...	17.5
4061.09	0.32	−0.34	...	...	...	...	...	48.0	...	...
4069.28	0.06	−0.33	...	22.7	...	...	39.1	21.1	16.0	43.3
4075.12	0.20	−0.40[e]	11.6	35.6*	22.4*	...	...	...	...	...
4116.77	0.06	−1.65	...	...	...	...	24.7	...	...	...
4133.36	0.32	−0.34	...	...	...	...	...	17.8	...	...
4156.08	0.18	0.10[f]	28.4	43.2*	...	...	...	...	...	...
4160.57	0.56	−0.45	...	...	...	...	25.6	...	...	...
4177.32	0.06	−0.04[e]	...	38.7*	...	22.5	61.7*	...	...	...
4358.17	0.32	−0.21	...	30.9	...	...	...	...	...	...
4446.39	0.20	−0.63	...	19.0	...	...	44.9	29.7	...	37.8
4462.99	0.56	−0.07	...	35.4	10.6	...	56.9	28.5	...	...
4516.36	0.32	−0.75	...	...	...	...	26.1	8.4	...	...
					Sm II					
3979.20	0.54	−0.19[g]	...	...	...	...	...	7.1	19.6	13.8
4064.58	0.33	−0.27[g]	...	...	...	...	19.5	...	...	...
4244.70	0.28	−0.73[h]	...	...	...	...	14.4	...	...	...
4318.94	0.28	−0.27	...	11.7	...	...	27.6	15.1	...	...
4424.34	0.49	0.07[g]	...	...	...	...	...	11.9	...	28.0
4434.32	0.38	−0.26	...	16.0	...	...	33.8	14.7	...	...
4467.34	0.66	0.12[i]	...	13.1	...	...	30.4	12.5	...	27.2
4499.48	0.25	−1.00[h]	...	...	...	...	23.6	...	...	...
4537.95	0.49	−0.23	...	...	...	...	30.5	...	...	...
4642.24	0.38	−0.52[h]	...	...	...	...	33.1	...	...	...

TABLE 2—*Continued*

Wavelength (Å)	LEP (eV)	log *gf*	29526−110	22898−027	31062−012	22880−074	31062−050	HD 196944	22942−019	30301−015
					Eu II					
3819.67	0.00	0.49[j]	55.6†	83.5†	19.1†	...	132.4†	43.4†	60.7†	...
3907.10	0.21	0.20	...	...	...	...	87.4†	15.4†	...	...
4129.70	0.00	0.20[j]	44.6†	55.7†	12.8†	...	116.0†	22.4†	40.5†	47.1†
4205.05	0.00	0.12[j]	33.7†	48.8†	8.7†	9.8†	...	21.1†	35.0†	...
					Dy II					
3944.68	0.00	0.08	...	28.3	...	11.9	...	32.7	34.9	48.1
4077.96	0.10	−0.03	...	31.0	...	...	53.4	...	...	...
					Er II					
3616.56	0.00	−0.33[k]	...	27.9	...	19.0	...	23.4	...	...
3786.84	0.00	−0.64	...	27.4	...	...	...	...	...	...
3830.48	0.00	−0.37[k]	...	43.7	...	...	...	...	...	...
3896.23	0.05	−0.24[k]	...	36.5	...	...	...	29.5	...	...
					Pb I					
3683.46	0.97	−0.52	30.1†	24.2†	...	...	45.3†	24.1†	...	26.2†
4057.82	1.32	−0.20	34.9†	27.4†	6.4†	15.4†	53.3†	24.5†	...	20.7†

NOTE.—Asterisks indicate lines that were not used in the analysis. Daggers indicate a synthesized value calculated for the abundance derived by spectrum synthesis; *gf*-values without a footnote are from Aoki et al. 2002b or 2001. Table 2 is also available in machine-readable form in the electronic edition of the *Astrophysical Journal*.

[a] Hannaford et al. 1982.
[b] Sneden et al. 1996.
[c] McWilliam 1998.
[d] Corliss & Bozman 1962, +0.23 dex.
[e] Cowley & Corliss 1983.
[f] Wiese & Martin 1980.
[g] Corliss & Bozman 1962, +0.49 dex.
[h] Biémont et al. 1989.
[i] Vogel et al. 1988.
[j] Biémont et al. 1982.
[k] Musiol & Labuz 1983.

non-LTE effects in the analysis of the Fe lines, which were neglected in the present work. For the purpose of error estimation, we therefore assume a larger uncertainty in the derived gravity for this star.

The carbon abundances were determined using the C_2 Swan bands for CS 31062−050, CS 22942−019, and CS 30301−015, stars for which the CH band at 4323 Å is too strong for abundance analysis. The line list produced by Aoki & Tsuji (1997) for C_2 Swan bands was applied. For the other five stars, the CH band was used for carbon abundance determination. The line positions of CH $A-X$ bands were calculated using the molecular constants derived by Zachwieja (1995) and the oscillator strengths of Brown (1987). Aoki et al. (2002a) showed that the carbon abundance derived from the C_2 band is by 0.2 dex higher than that from the CH band for LP 625-44, indicating that we should include this additional uncertainty of about 0.2 dex for the carbon abundances. The CN 3883 Å feature was used for estimates of nitrogen abundances. The line positions of the CN violet system were calculated using the

TABLE 3
STELLAR PARAMETERS

Star	$T_{\rm eff}$ (K)	log g	$v_{\rm tur}$ (km s^{-1})	[Fe/H]	[C/Fe]	[N/Fe]
CS 29526−110	6500[a]	3.2	1.6	−2.38	2.2	1.4:
CS 22898−027	6250[a,b]	3.7	1.5	−2.25	2.2	0.9
CS 31062−012	6250[a]	4.5	1.5	−2.55	2.1	1.2
CS 22880−074	5850[a]	3.8	1.4	−1.93	1.3	−0.1:
CS 31062−050	5600[a,b]	3.0	1.3	−2.32	2.0	1.2
HD 196944.....	5250[a]	1.8	1.7	−2.25	1.2	1.3
CS 22942−019	5000[a]	2.4	2.1	−2.64	2.0	0.3
CS 30301−015	4750[a]	0.8	2.2	−2.64	1.6	0.6:

[a] Based on the $(B-V)_0$ color indices.
[b] Based on the $(V-K)_0$ color indices.

molecular constants presented by Prasad & Bernath (1992) and the oscillator strengths of Bauschlicher, Langhoff, & Taylor (1988). Unfortunately, the nitrogen abundances of CS 29526−110, CS 22880−074, and CS 30301−015 are unreliable because the CN band is either too weak or too strong for abundance determination. The results of the carbon and nitrogen abundances are also given in Table 3. The oxygen abundances are assumed to be [O/Fe] = 0.5 in the analysis, taking account of the well-known overabundances of oxygen found in metal-poor stars. The derived carbon and nitrogen abundances are not sensitive to the oxygen abundances assumed in the analysis for warm ($T_{\rm eff} \gtrsim 5000$ K) stars because the fraction of carbon bound in the CO molecule is small. The effect of the assumption for the oxygen abundance most severely appears in CS 30301−015 ($T_{\rm eff} = 4750$ K); we tested the range $0.0 < [{\rm O/Fe}] < 1.5$ for this star but found that the effect on abundance determination for carbon and nitrogen is smaller than 0.1 dex.

The Pb I λ4057 line was detected for seven stars in our sample. Figure 1 shows examples of the observed spectra and the results of synthetic fits for HD 196944 and CS 31062−050. In this analysis we adopted the line data for the hyperfine splitting and isotope shifts determined by Simons et al. (1989), as given in Table 4. We found that the fit between the observed spectra and the calculated ones is better when the absolute wavelength of the Pb lines is slightly shifted. For this reason, we shifted the wavelength of these lines by 0.005 Å, which is as large as the uncertainty in the determination of the absolute line position by Simons et al. (1989), in our spectrum synthesis. The CH λ4057 line blending with the Pb I line was calculated for the carbon abundance that best reproduced other lines of the same CH band. Therefore, the errors in carbon abundances due to the uncertainties of oscillator strengths of the band system do not directly affect the spectrum synthesis for the Pb I λ4057 line.

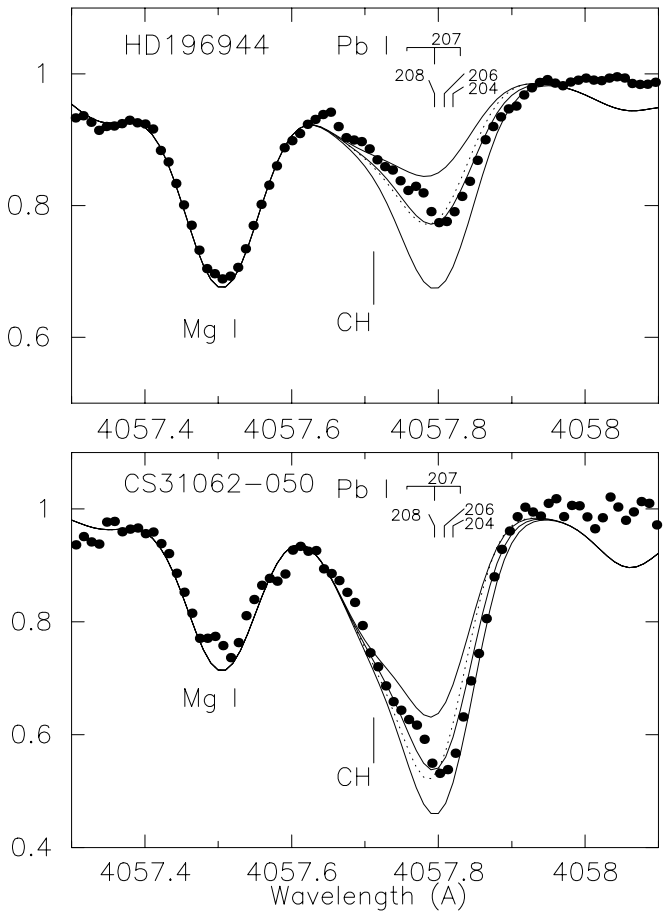

FIG. 1.—Comparison of the observed spectra (*filled circles*) and synthetic spectra (*lines*) near the Pb I λ4057.8 line for HD 196944 and CS 31062−050. Solid lines show the synthetic spectra assuming the solar system Pb isotope ratio (see text). The Pb abundances assumed in the calculations are [Pb/Fe] = 1.6, 1.9, and 2.2 for HD 196944 and [Pb/Fe] = 2.6, 2.9, and 3.2 for CS 31062−050. The dotted lines show the synthetic spectra calculated with a single line approximation for [Pb/Fe] = 1.9 and 3.1 for HD 196944 and CS 31062−050, respectively.

TABLE 4
HYPERFINE AND ISOTOPE SPLITTING OF Pb λ4057.8

Wavelength (Å)	Fraction	Isotope
4057.7524.....	0.015	207b
4057.7895.....	0.135	207a
4057.7895.....	0.524	208
4057.8030.....	0.236	206
4057.8150.....	0.015	204
4057.8251.....	0.075	207c

The effects of hyperfine splitting and isotope shifts were included, assuming the solar system isotope ratio for Pb (see Aoki et al. 2001). However, this assumption may not be appropriate for the very metal-poor stars studied here. For instance, a large production of ^{208}Pb was predicted for the *s*-process at low metallicity (see, e.g., Gallino et al. 1998). In order to estimate the uncertainty of the Pb abundance due to the effect of the isotope ratio assumed, we also tried the analysis with a single line approximation for the Pb I λ4057 line, which simulates the case in which ^{208}Pb is dominant over the other isotopes. The synthetic spectra calculated with the single line approximation are shown by dotted lines in Figure 1. Because of the larger effect of saturation of the absorption, the derived Pb abundance from the single line approximation is larger than that from the analysis including isotope shifts with the assumption of the solar system isotope ratio. The difference of the resulting abundance is about 0.2 dex for CS 31062−050, in which the Pb I λ4057 line is strongest among our objects. The effect of the isotope ratios assumed in the analysis for other objects is about 0.1 dex or smaller. We include these uncertainties in the error estimates below.

We found that the abundances of the lighter neutron-capture elements (e.g., Ba), as well as the stellar parameters, of CS 31062−050 are quite similar to those of the well-studied object LP 625-44. However, the Pb absorption line in CS 31062−050 is significantly stronger than that of LP 625-44 (see Fig. 6 of Aoki et al. 2002b). This clearly indicates a large dispersion in the ratio of the abundances between the lighter *s*-process elements and Pb.

The Pb I λ3683 line was also detected in five of the above seven stars. Although the quality of the spectra at 3683 Å is worse than that at 4057 Å, we found that the abundances derived from the 3683 Å line agree well with those obtained from the 4057 Å line within the errors. We note that the abundances based on the 4057 Å line were adopted as the final result given in Table 5; those based on the 3683 Å line

TABLE 5
[Fe/H] AND RELATIVE ABUNDANCE [X/Fe]

	CS 29526−110				CS 22898−027				CS 31062−012				CS 22880−074			
Ion	[X/Fe][a]	log ϵ	n[b]	Standard Error	[X/Fe][a]	log ϵ	n[b]	s.e.	[X/Fe][a]	log ϵ	n[b]	Standard Error	[X/Fe][a]	log ϵ	n[b]	s.e.
Fe I.....	−2.38	5.12	34	0.16	−2.26	5.24	36	0.11	−2.55	4.95	55	0.11	−1.93	5.57	58	0.11
Fe II....	−2.38	5.12	6	0.20	−2.25	5.25	4	0.16	−2.55	4.95	3	0.15	−1.93	5.57	11	0.14
Sr II	0.88	1.42	2	0.43	0.92	1.59	2	0.41	0.30	0.67	2	0.40	0.39	1.38	2	0.40
Y II.....	...	...	...	...	0.73	0.71	2	0.20	0.59	0.27	1	0.20	0.16	0.46	2	0.18
Zr II....	1.11	1.34	1	0.23	1.01	1.37	2	0.17	...	...	...	...	...	...	...	...
Ba II ...	2.11	1.95	2	0.17	2.23	2.20	3	0.14	1.98	1.65	1	0.16	1.31	1.60	1	0.16
La II ...	1.69	0.53	6	0.24	2.13	1.10	5	0.18	2.02	0.69	3	0.18	1.07	0.36	3	0.18
Ce II ...	2.01:	1.26:	1	0.22	2.13	1.51	18	0.13	2.12	1.20	7	0.13	1.22	0.92	3	0.14
Nd II...	2.01	1.12	2	0.23	2.23	1.47	8	0.14	1.79	0.73	4	0.14	1.20	0.76	1	0.18
Sm II...	...	...	...	...	2.08	0.82	3	0.15	...	...	...	...	...	...	...	...
Eu II ...	1.73	−0.10	3	0.20	1.88	0.18	3	0.15	1.62	−0.38	3	0.14	0.5	−0.8	1	0.17
Dy II...	...	...	...	...	1.78	0.70	2	0.17	...	...	...	...	0.60	−0.16	1	0.19
Er II....	...	...	...	...	2.40	1.12	4	0.17	...	...	...	...	1.41	0.45	1	0.19
Pb II ...	3.3	3.0	2	0.24	2.84	2.65	2	0.19	2.4	1.9	1	0.19	1.9	2.0	1	0.19

	CS 31062−050				HD 196944				CS 22942−019				CS 30301−015			
Ion	[X/Fe][a]	log ϵ	n[b]	Standard Error	[X/Fe][a]	log ϵ	n[b]	s.e.	[X/Fe][a]	log ϵ	n[b]	Standard Error	[X/Fe][a]	log ϵ	n[b]	s.e.
Fe I.....	−2.31	5.19	26	0.14	−2.25	5.25	76	0.19	−2.64	4.86	18	0.14	−2.64	4.86	30	0.18
Fe II....	−2.33	5.17	3	0.16	−2.26	5.24	10	0.20	−2.64	4.86	3	0.15	−2.63	4.87	9	0.15
Sr II	0.91	1.51	2	0.18	0.84	1.51	3	0.22	1.7:	2.0:	2	0.17	0.3:	0.6:	1	0.23
Y II.....	...	...	...	...	0.56	0.54	7	0.22	1.58	1.17	2	0.18	0.29	−0.12	4	0.20
Zr II....	1.02	1.31	2	0.16	0.66	1.02	6	0.20	1.69	1.66	3	0.15	...	...	...	...
Ba II ...	2.30	2.21	2	0.15	1.10	1.07	3	0.19	1.92	1.50	3	0.13	1.45	1.03	1	0.16
La II ...	2.44	1.34	4	0.20	0.91	−0.12	6	0.28	1.20	−0.24	2	0.26	0.84	−0.58	3	0.25
Ce II ...	2.10:	1.41	22	0.12	1.01	0.39	30	0.19	1.54	0.53	6	0.12	1.16	0.15	14	0.15
Nd II...	2.24	1.41	15	0.12	0.86	0.10	16	0.20	1.26	0.11	7	0.12	1.25	−0.42	3	0.17
Sm II...	2.15	0.81	8	0.16	0.78	−0.49	5	0.23	1.64	−0.02	1	0.18	0.85	−0.81	3	0.20
Eu II ...	1.84	0.07	3	0.13	0.17	−1.53	4	0.19	0.79	−1.30	3	0.12	0.2:	−1.9:	1	0.18
Dy II...	2.08	0.93	1	0.17	0.46	−0.62	1	0.17	0.84	−0.63	1	0.15	0.57	−0.90	1	0.20
Er II....	...	...	...	...	0.81	−0.47	2	0.22	...	...	...	...	...	...	...	...
Pb II ...	2.9	2.6	2	0.24	1.9	1.7	2	0.24	$\leq$1.6	$\leq$1.0	2	...	1.7	1.1	2	0.24

[a] The value of [Fe/H] is given for Fe I and Fe II.
[b] The number of lines used for the analysis.

were only used for confirmation. An upper limit on the Pb abundance was obtained for CS 22942−019, in which the above Pb lines were not detected.

The abundances of most of the other neutron-capture elements were determined by standard analysis based on the measured equivalent widths, while the abundances of Ba and Eu were determined from spectrum synthesis. The effects of hyperfine splitting and isotope shifts were included in the analysis of Ba, La, Nd, and Eu lines using the line lists of McWilliam (1998) and Aoki et al. (2001).

In order to estimate the random error in the analysis, we first calculated the dispersion of the abundances for individual Fe I lines in each star. In addition, we assumed the random error in *gf*-values to be 0.1 dex and added it in quadrature to the above dispersion. The random error was evaluated by dividing this estimate by $n^{1/2}$ (n is the number of lines used in the analysis) for each neutron-capture element. For Pb abundances, we also included the uncertainties due to the isotope ratio assumed in the spectrum synthesis (0.2 dex for CS 31062−050 and 0.1 dex for other stars). The errors in the abundance determination from the uncertainties of the atmospheric parameters were evaluated for $\sigma(T_{\rm eff}) = 100$ K, $\sigma(\log g) = 0.3$, and $\sigma(v) = 0.5$ km s^{-1} for HD 196944 and CS 22898−027. These results were then applied to four of the remaining stars. We assumed $\sigma(T_{\rm eff}) = 200$ K for CS 29526−110 and CS 30301−015 and $\sigma(\log g) = 0.5$ for CS 29526−110, taking the uncertainties noted above into consideration. We finally derived the total uncertainty by adding in quadrature the individual errors and list them in Table 5.

We also tried to estimate the effective temperatures for seven stars in our sample based on the Balmer line strengths measured from the medium-resolution spectra obtained during the HK survey follow-up. These effective temperatures are systematically lower, by about 300 K, than those derived above from the broadband colors. The effects of the changes of effective temperature by −300 K on the resulting [Fe/H] and [Pb/Ba], which will be discussed below, are about −0.20 and 0.25 dex, respectively. Although these effects are important in the determination of the abundances and will be investigated more thoroughly in our future work, the systematic shift of the abundance ratios does not change the following discussion on the dispersion in the values of [Pb/Ba] found in our sample.

The abundances of HD 196944 derived in this work generally agree with those by Začs, Nissen, & Schuster (1998)

for iron and carbon and van Eck et al. (2001) for other elements, including Pb, within 0.2 dex, except for La (our result is 0.38 dex higher than that of van Eck et al. 2001). The agreement between the abundances of HD 196944 determined by van Eck et al. (2001) and those obtained in the present analysis (following the previous work for LP 625-44) indicates that the significant difference in the abundance ratios of Pb, as compared to the lighter *s*-process elements, in the objects analyzed by van Eck et al. (2001) and those by Aoki et al. (2001) is not due to differences in the respective analysis procedures.

4. DISCUSSION AND CONCLUDING REMARKS

The resulting abundances for two of the stars in our sample are shown in Figure 2 along with the scaled abundance patterns of solar system material, the main *s*-process component, and the (inferred) *r*-process pattern (Arlandini et al. 1999). These comparisons are useful to distinguish the origins of the neutron-capture elements detected in our objects. The abundance patterns of elements with $56 \leq Z \leq 63$ in our stars agree with the *s*-process pattern much better than with the *r*-process pattern. This result implies that, as expected, the neutron-capture elements in our stars principally originate in the *s*-process. The values of [Ba/Eu] for four of the stars in our sample (CS 29526−110, CS 22898−027, CS 31062−012, and CS 31062−050) are significantly lower ([Ba/Eu] = 0.36–0.47) than seen in the main *s*-process component ([Ba/Eu] = 1.15; Arlandini et al. 1999). We suggest, however, that the derived abundance ratios of [Ba/Eu] have been produced by an *s*-process that produces *different* abundance ratios from that of the main *s*-process component. Indeed, Goriely & Mowlavi (2000) predicted lower values of [Ba/Eu] (∼0.4) for yields of metal-deficient AGB stars, although the [Ba/Eu] value of our objects is not correlated with metallicity. To explain these low values of [Ba/Eu] by the mixture of the abundance ratios of the *r*- and *s*-process components in the solar system, we must assume that about 80%–90% of Eu nuclei were produced by the *r*-process. If this were true, it follows that these four stars show very large excesses of their *r*-process elements ([Eu/Fe] = 1.5–1.8), similar to CS 31082−001, an extreme *r*-process element–enhanced star (Cayrel et al. 2001; Hill et al. 2002). However, recent high-resolution studies of metal-poor giants indicate that stars with such large excesses of *r*-process elements are quite rare. An ongoing survey by N. Christlieb et al. (2002, in preparation) confirms the original suggestion by T. C. Beers (2000, private communication) that roughly 3% of giants with [Fe/H] < −2.5 exhibit [*r*/Fe] ≥ 1.0. Hence, it would be difficult to appeal to this explanation to account for the excesses of Eu in the four stars in our sample. We treat our stars as having the abundance patterns produced by the *s*-process for neutron-capture elements in this paper because the elements discussed below (Ba and Pb) should principally originate from the *s*-process, even though *r*-process contamination may have contributed to a portion of the observed Eu excesses.

Figure 3 shows the ratio [Pb/Ba], representing the ratio of abundances between elements located at the second and third *s*-process peaks, as a function of metallicity ([Fe/H]). There exists a large scatter in [Pb/Ba] for these stars, larger than can be accounted for by the errors in the abundance analysis. It is not apparent that our stars can be readily classified into separate groups on the basis of the present data. There may be evidence for an decreasing trend of [Pb/Ba]

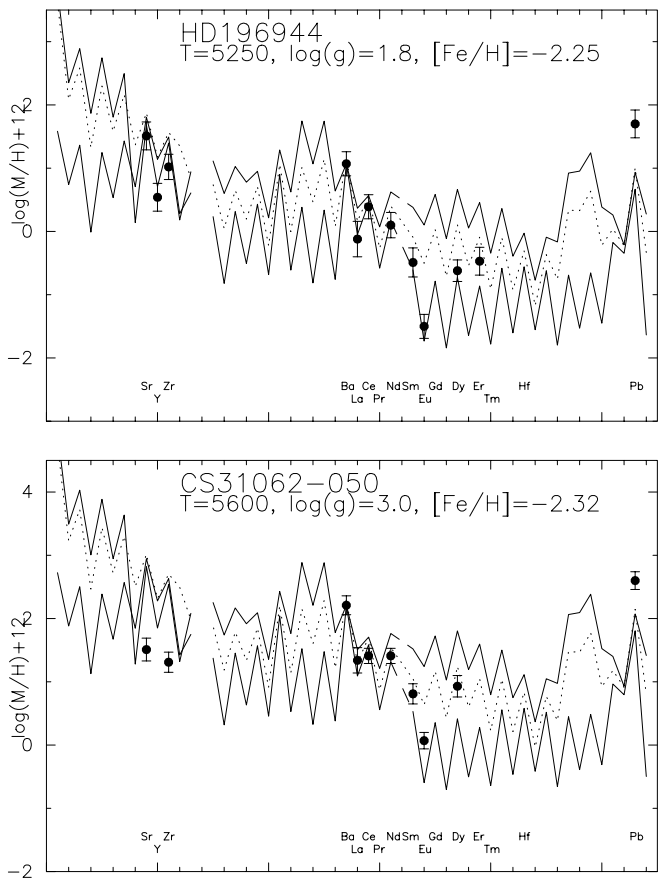

FIG. 2.—Abundances of heavy elements as a function of atomic species for HD 196944 (*top*) and CS 31062−050 (*bottom*). The thick solid line indicates the main *s*-process component determined by Arlandini et al. (1999), while the thin line indicates the *r*-process component. The dotted line represents the total solar abundance adopted in Arlandini et al. (1999). All abundance patterns are normalized to the observed Ba abundances.

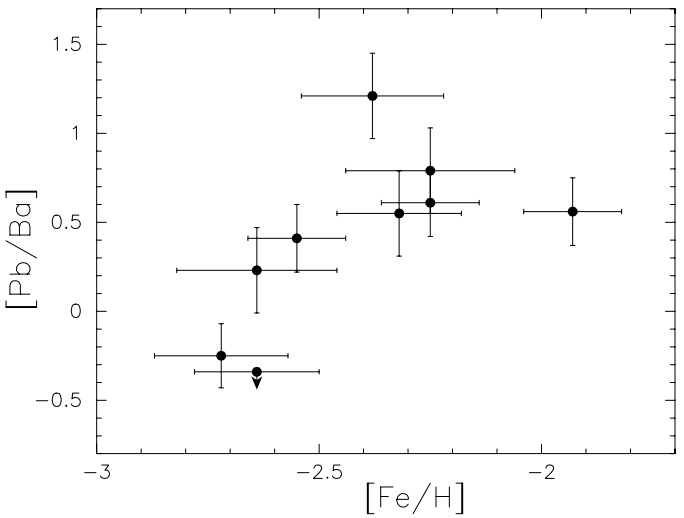

FIG. 3.—[Pb/Ba] as a function of [Fe/H]. Filled circles show the results of the present work and of Aoki et al. (2002b) for LP 625-44 based on the Subaru/HDS spectra.

with decreasing [Fe/H] (the correlation estimated from objects in Fig. 3, excluding CS 22942−019, is represented as $[Pb/Ba] = 2.74 + 0.93[Fe/H]$ with the standard error of the slope of 0.56, i.e., the possible slope is significant at the 1.7 σ level). Additional data will presumably help to clarify these questions. Additional studies of *s*-process nucleosynthesis at low metallicity should be carried out to explore the possible reasons for this large dispersion and the possible dependence on metallicity of the Pb/Ba ratios.

Comparison of these results with the predictions of AGB nucleosynthesis models of Gallino et al. (1998) and Busso, Gallino, & Wasserburg (1999) provides a constraint on their ^{13}C pocket models.[8] Figure 1 of Ryan et al. (2001) shows the metallicity dependence of [Pb/Fe] and [Ba/Fe] predicted by the model for 1.5 $M_\odot$ AGB stars, compared with the abundance ratios observed in LP 625-44. The value of [Pb/Ba] is sensitive to the adopted ^{13}C profile, represented by the normalization factor of the ^{13}C pocket in the standard model of Busso et al. (1999). The [Pb/Ba] values found in our stars with $-2.7 \leq [Fe/H] \leq -1.9$ distribute from −0.3 to 1.2 (Fig. 3). This range of the abundance ratios is not explained by the standard model, which predicts $[Pb/Ba] \sim 2$, but can be explained by models where the amount of ^{13}C produced as the neutron source for the *s*-process is lowered by factors of 6–24 relative to the standard model.

We would also like to mention the model of the *s*-process in AGB stars recently proposed by Iwamoto et al. (2002). Their model for AGB stars with $[Fe/H] = -2.7$ and $M = 2$ $M_\odot$ shows a possible production of ^{13}C, a candidate for the neutron source of the *s*-process, as the result of proton mixing into the hot He shell at the second thermal pulse (see also Fujimoto, Ikeda, & Iben 2000). Since the value of neutron exposure predicted by their model is rather high ($\tau \sim 1$ mb^{-1}), one may expect high Pb abundances relative to those of lighter neutron-capture elements. However, the small number of the exposures (only one in their model) is preferable to account for the low Pb abundances that we find in some stars in our sample (Aoki et al. 2001). This mechanism for producing the required free neutrons is expected to occur only in very metal-poor ($[Fe/H] \lesssim -2.5$) AGB stars and may explain the abundances of some objects with lower metallicity and high [Pb/Ba] values. The comparison with this model is, however, still quite speculative, and further theoretical study for the possibility of flash-driven proton mixing and its contribution to the *s*-process is required.

Finally, we point out that clear temporal variations of radial velocity, which directly imply the binarity of the object, have thus far been detected for only three of the carbon-enhanced, metal-poor stars we have been studying in recent years: CS 22942−019 (Preston & Sneden 2001), CS 29526−110 (§ 2), and LP 625-44 (Aoki et al. 2000). Preston & Sneden (2001) reported that *none* of the three carbon-rich, metal-poor subgiants in their sample, including the stars CS 22898−027 and CS 22880−074 studied here, exhibited radial velocity variations exceeding 0.5 km s^{-1} over an 8 yr period. Furthermore, no radial velocity variation has been found for the subgiant (or dwarf) LP 706-7 (Norris et al. 1997). These results suggest that the enhancement of neutron-capture elements in these subgiants may not be explained as a result of the transfer of material rich in *s*-process elements across a binary system including an AGB star. For comparisons with the predictions of AGB models, confirmation of binarity based on the radial velocity monitoring is strongly desired. It is interesting to note the large dispersion of [Pb/Ba] values of the three objects (CS 22942−019, CS 29526−110, and LP 625-44) for which the variation of radial velocity have been observed. This suggests that the Pb/Ba ratios produced by *s*-process nucleosynthesis in metal-deficient AGB stars show a large scatter, although the sample is still too small to be confident in this regard.

The present work clearly shows a variety in the abundance ratios of neutron-capture elements for carbon-rich, metal-poor stars and underscores the importance of further studies for individual objects, including long-term radial velocity monitoring, for development of a better understanding of heavy-element production by the *s*-process operating at low metallicity.

The authors are pleased to acknowledge valuable discussions with R. Gallino and M. Busso on the variation of *s*-process nucleosynthesis in their Population II AGB models. We would also like to thank the anonymous referee for useful comments for improving this paper. T. C. B. acknowledges partial support for this work from grant AST 00-98549, awarded by the US National Science Foundation.

[8] Uncertainties in the amount of ^{13}C in the pocket reflects the unknown amount of mixing of protons from the H-rich envelope down into the C-rich zone. Recent model calculations by Cristallo et al. (2001; see also Goriely & Mowlavi 2000) treat the proton mixing as an input parameter rather than the amount of ^{13}C in the "pocket." The efficiency of the ^{13}C as a neutron source for the *s*-process is also affected by the profile of neutron poisons like ^{14}N.

REFERENCES

Alonso, A., Arribas, S., & Martínez-Roger, C. 1996, A&A, 313, 873
Aoki, W., Norris, J. E., Ryan, S. G., Beers, T. C., & Ando, H. 2000, ApJ, 536, L97
———. 2002a, ApJ, 567, 1166
Aoki, W., & Tsuji, T. 1997, A&A, 317, 845
Aoki, W., et al. 2001, ApJ, 561, 346
———. 2002b, PASJ, 54, 427
Arlandini, C., Käppeler, F., Wisshak, K., Gallino, R., Lugaro, M., Busso, M., & Straniero, O. 1999, ApJ, 525, 886
Bauschlicher, C. W., Langhoff, S. R., & Taylor, P. R. 1988, ApJ, 332, 531
Beers, T. C. 1999, in ASP Conf. Ser. 165, Third Stromlo Meeting: The Galactic Halo, ed. B. Gibson, T. Axelrod, & M. Putman (San Francisco: ASP), 202
Beers, T. C., Preston, G. W., & Shectman, S. A. 1992, AJ, 103, 1987
Biémont, E., Grevesse, N., Hannaford, P., & Lowe, R. M. 1989, A&A, 222, 307
Biémont, E., Karner, C., Meyer, G., Träger, F., & zu Putlitz, G. 1982, A&A, 107, 166
Brown, J. A. 1987, ApJ, 317, 701
Busso, M., Gallino, R., Lambert, D. L., Travaglio, C., & Smith, V. V. 2001, ApJ, 557, 802
Busso, M., Gallino, R., & Wasserburg, G. J. 1999, ARA&A, 37, 239
Cayrel, R., et al. 2001, Nature, 409, 691
Corliss, C. H., & Bozman, W. R. 1962, Experimental Transition Probabilities for Spectral Lines of Seventy Elements (NBS Monogr. 53; Washington: GPO)
Cowley, C. R., & Corliss, C. H. 1983, MNRAS, 203, 651
Cristallo, S., Straniero, O., Gallino, R., Herwig, F., Chieffi, A., Limongi, M., & Busso, M. 2001, Nucl. Phys. A, 688, 217
Fujimoto, M. Y., Ikeda, Y., & Iben, I. 2000, ApJ, 529, L25
Gallino, R., Arlandini, C., Busso, M., Lugaro, M., Travaglio, C., Straniero, O., Chieffi, A., & Limongi, M. 1998, ApJ, 497, 388
Goriely, S., & Arnould, M. 2001, A&A, 379, 1113
Goriely, S., & Mowlavi, N. 2000, A&A, 362, 599
Hannaford, P., Lowe, R. M., Grevesse, N., Biémont, E., & Whaling, W. 1982, ApJ, 261, 736
Hill, V., et al. 2002, A&A, 387, 560
Iwamoto, N., Kajino, T., Mathews, G. J., Fujimoto, M. Y., & Aoki, W. 2002, J. Nucl. Sci. Tech., in press

Käppeler, F., Beer, H., & Wisshak, K. 1989, Rep. Prog. Phys., 52, 945
Kurucz, R. L. 1993, CD-ROM 13, ATLAS9 Stellar Atmospheres Programs and 2km/s Grid (Cambridge: SAO)
McWilliam, A. 1998, AJ, 115, 1640
Musiol, K., & Labuz, S. 1983, Phys. Scr., 27, 422
Noguchi, K., et al. 2002, PASJ, submitted
Norris, J. E., Ryan, S. G., & Beers, T. C. 1997, ApJ, 488, 350
———. 1999, ApJS, 123, 639
Prasad, C. V. V., & Bernath, P. F. 1992, J. Mol. Spectrosc., 156, 327
Preston, G. W., & Sneden, C. 2001, AJ, 122, 1545
Ryan, S. G., Aoki, W., Norris, J. E., Beers, T. C., Gallino, R., Busso, M., & Ando, H. 2001, Nucl. Phys. A, 688, 209
Schatz, H., Toenjes, R., Pfeiffer, B., Beers, T. C., Cowan, J. J., Hill, V., & Kratz, K.-L. 2002, ApJ, submitted
Simons, J. W., Palmer, B. A., Hof, D. E., & Oldenborg, R. C. 1989, J. Opt. Soc. Am. B, 6, 1097
Skrutskie, M. F., et al. 1997, in The Impact of Large Scale Near-IR Sky Surveys, ed. F. Garzón (Dordrecht: Kluwer), 187
Sneden, C., McWilliam, A., Preston, G. W., Cowan, J. J., Burris, D., & Armosky, B. J. 1996, ApJ, 467, 819
Travaglio, C., Gallino, R., Busso, M., & Gratton, R. 2001, ApJ, 549, 346
van Eck, S., Goriely, S., Jorissen, A., & Plez, B. 2001, Nature, 412, 793
Vogel, O., Edvardsson, B., Wannstrom, A., Arnesen, A., & Hallin, R. 1988, Phys. Scr., 38, 567
Wiese, W. L., & Martin, G. A. 1980, Wavelengths and Transition Probabilities for Atoms and Atomic Ions, NSRDS-NBS No. 68, Part II (Washington: GPO)
Zachwieja, M. 1995, J. Mol. Spectrosc., 170, 285
Začs, L., Nissen, P. E., & Schuster, W. J. 1998, A&A, 337, 216